

Toward Neuronal Implementations of Delayed Optimal Control

Jing Shuang (Lisa) Li

Abstract—Animal sensorimotor behavior is frequently modeled using optimal controllers. However, it is unclear how the neuronal circuits within the animal’s nervous system implement optimal controller-like behavior. In this work, we study the question of implementing a delayed linear quadratic regulator with linear dynamical “neurons” on a muscle model. We show that for any second-order controller, there are three minimal neural circuit configurations that implement the same controller. Furthermore, the firing rate characteristics of each circuit can vary drastically, even as the overall controller behavior is preserved. Along the way, we introduce concepts that bridge controller realizations to neural implementations that are compatible with known neuronal delay structures.

I. INTRODUCTION AND MOTIVATION

Control theory — particularly, linear optimal control — has emerged as the leading framework for sensorimotor modeling of various species and behaviors [1]–[5]. These works typically focus on modeling input-output behaviors using a parameterized controller (e.g. a linear quadratic regulator), tuning parameters (e.g. state and input penalty) to match data (e.g. movement trajectories, muscle forces) when available. Most models do not consider the underlying implementation of these input-output behaviors. Indeed, this is a common criticism of controls-based models — that they capture behavior without revealing the underlying implementation [6], [7].

Current approaches to relate controller behavior to implementation roughly fall into two categories: anatomy-centered and learning-centered. In anatomy-centered approaches, neuroscientists attempt to associate parts of the controller (e.g. internal model) with specific parts of the brain [4], [8], [9]. In learning-centered approaches, computer scientists create neurally-plausible approximations of controllers by tuning networks of neurons or training them on controller tasks [10]–[12]. More recently, control theorists have joined the fray, drawing parallels between controller connectivity patterns and neuronal connectivity patterns [13]–[15]. All of these approaches have a common feature: they focus on one specific implementation of the controller. However, a given transfer function has many potential realizations; similarly, a given controller can be implemented in multiple ways. This is a longstanding observation in both control theory and in neuroscience [16], but we do not yet have tools to rigorously explore the non-unique relationship between behavior and implementation in the neuroscience setting. The primary goal of this paper is to begin to address this research gap. Figure

1 summarizes behavior and implementation in the context of neuroscience and control theory.

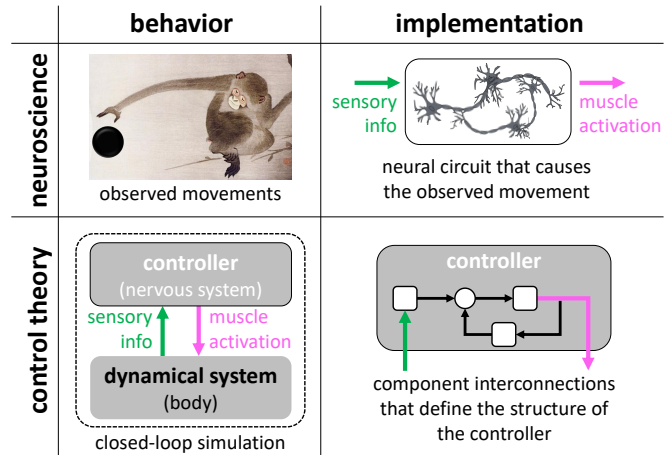


Fig. 1. Behavior vs. implementation in neuroscience and in control theory. While control theory offers explanations for behaviors seen in neuroscience experiments, it currently offers few explanations for neural circuitry (i.e. implementation) underlying these behaviors.

We focus on delayed optimal controllers [13], [15], which incorporate conduction delays of neurons (Section III). We introduce necessary concepts that translate controller realizations to neural circuits (Section IV), and study different circuits associated with a given controller (Sections V and VI). Throughout the paper, we ground our discussions in a simple neuromuscular example (Section II). However, the general methods presented extend to arbitrary linear time-invariant discrete-time systems. We conclude with some promising avenues of future investigation (Section VII).

II. PROBLEM SETUP

When using control theory to create models for neuroscience, we must first define what constitutes the controller, and what dynamical system this controller acts upon. Here, our controller is the nervous system, which acts upon a muscle subject to muscle dynamics. The nervous system receives information about the force of the muscle from the Golgi tendon organ, which is a sensor located on the muscle. The nervous system elicits force production from the muscle through muscle activation — a motorneuron outputs some firing rate to the muscle, which responds accordingly. The overall system is depicted in Figure 2. This framing of the system allows us to compare controllers to neuronal circuits within the nervous system.

The nervous system is made of many neurons — on the order of 10^{10} neurons for humans, and on the order of 10^5

J.S.L. is with the Department of Electrical Engineering and Computer Science at the University of Michigan, Ann Arbor. jslisali@umich.edu.

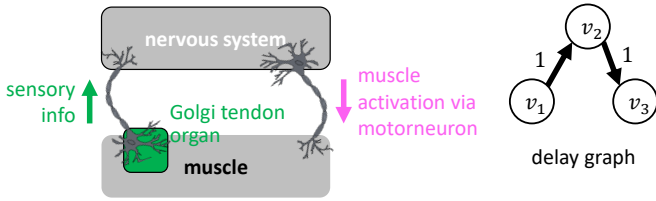


Fig. 2. (Left) The neuromuscular control system; the muscle is the ‘plant’, and the nervous system is the ‘controller’. The Golgi tendon organ senses the muscle force and communicates this to the nervous system, which fires a motoneuron to induce muscle activation. (Right) Delay graph associated with the neuromuscular control system. There is a delay of 1 timestep from v_1 (the Golgi tendon organ) to v_2 (the nervous system), and a delay of 1 timestep from v_2 to v_3 (the muscle). No other communication paths exist between the three vertices.

neurons for something as small as a fruit fly. How many neurons are involved in neuromuscular control depends on the motor task. Simple tasks, such as the one in this work, are typically carried out in spinal circuits which use relatively few neurons; conversely, complex tasks may involve many neurons across both the brain and spine.

We use a muscle model from [17]¹. The model is written as:

$$\frac{df(t)}{dt} = \frac{f_{\max}}{\tau(1 + e^{-r(t)})} - \frac{f(t)}{\tau} \quad (1)$$

where $f(t)$ is a scalar function representing muscle force, and $r(t)$ represents the firing rate of the motoneuron; both are time-varying signals. f_{\max} and τ are parameters representing the maximum force output of the muscle and the time-constant of the muscle. When the motoneuron is not firing, the muscle force decays; when the motoneuron fires at a constant rate, the muscle force rises to some fraction of the maximum muscle force.

We convert this system to a linear discrete-time system. First, we linearize about some equilibrium point (\bar{f}, \bar{u}) , and define the new state and input variables $\delta_f := f - \bar{f}$ and $\delta_r := r - \bar{r}$. Then, we discretize the system with some sampling time T_s to obtain:

$$\delta_f(t+1) = A\delta_f(t) + B\delta_r(t) \quad (2)$$

An example of the open-loop input response of the linearized muscle system is shown in Figure 3.

In animals, both sensing and actuation are subject to neuronal conduction delay. For instance, on a human, a sensory signal from a muscle on the foot must travel from the foot to the spine, and an actuation signal must travel from the spine back to the foot. Typical values are on the order of 10 ms each way [18]. Even for animals much smaller than humans (e.g. fruit flies), conduction values are still comparable [19] — though neural signals have a shorter distance to travel in smaller animals, they typically travel on

¹Note: the model in [17] includes two dimensionless parameters D_0 and D_1 , which are randomized and represent different activation characteristics. In this work, we use $D_0 = 0$, $D_1 = 1$, which are within the biologically plausible range and allow for simple equations. The general findings in this paper do not change if we change these values, though the algebra will be slightly more complicated

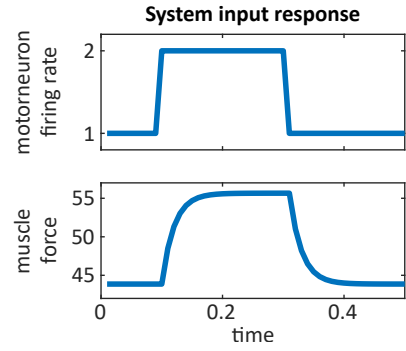


Fig. 3. Open-loop response of muscle forcing to motoneuron firing rate in the linear discrete-time model. An increase in firing rate results in an increase of muscle force (with some transient dynamics); similarly, decreased firing rate results in decreased force.

smaller and therefore slower nerves and axons. To include delay in our formulation, we can write our controller as:

$$\delta_r(t) = \mathcal{K}(\delta_f(0 : t - T)) \quad (3)$$

where \mathcal{K} is a linear map that depends on past values of its input, and T is a non-negative integer denoting net sensorimotor delay (i.e. the sum of delays to and from the nervous system). In frequency-domain terms, let $\Delta_f(z) := \mathcal{Z}(\delta_f(t))$ and $\Delta_r(z) := \mathcal{Z}(\delta_r(t))$ where \mathcal{Z} is the Z-transform. The transfer function $G(z) := \frac{\Delta_r(z)}{\Delta_f(z)}$ should have a relative degree of at least T , i.e. the difference between the denominator polynomial degree and numerator polynomial degree should be greater than or equal to T .

III. OPTIMAL DELAYED CONTROLLER

We now seek a delayed controller of the form (3) that is LQ-optimal. The LQ cost is

$$J = \sum_{t=0}^{\infty} \delta_f(t)^\top Q \delta_f(t) + \delta_r(t)^\top R \delta_r(t) \quad (4)$$

where Q and R are the penalty matrices for state and input, respectively.

We will use methods from previous work [13] to construct this controller. For simplicity, we assume that the system has been discretized so that there is one timestep of communication delay from controller to actuator, and one timestep from sensor to controller, i.e. net sensorimotor delay is $T = 2$. Starting with system (2), we introduce two new variables:

$$\begin{aligned} \gamma(t+1) &= \mu(t) \\ \delta_r(t+1) &= \gamma(t) \end{aligned} \quad (5)$$

where the variable μ represents *intended* actuation, which is delayed by two timesteps before it reaches the physical system as δ_r . γ is a virtual signal representing the intended actuation at varying intermediate delays — if the delay is larger than one timestep, then we will have multiple virtual signals. We now introduce augmented state vector

$$\chi(t) := \begin{bmatrix} \delta_f(t) \\ \gamma(t) \\ \delta_r(t) \end{bmatrix} \quad (6)$$

We can then write augmented state equations

$$\chi(t+1) = \tilde{A}\chi(t) + \tilde{B}\mu(t) \quad (7)$$

where

$$\tilde{A} = \begin{bmatrix} A & 0 & B \\ 0 & 0 & 0 \\ 0 & I & 0 \end{bmatrix}, \quad \tilde{B} = \begin{bmatrix} 0 \\ I \\ 0 \end{bmatrix} \quad (8)$$

Equations for systems with more delays are provided in [13].

The LQ cost can be rewritten in terms of the augmented state as:

$$J = \sum_{t=0}^{\infty} \tilde{x}(t)^\top \tilde{Q} \tilde{x}(t) \quad (9)$$

where $\tilde{Q} = \text{diag}(Q, 0, R)$. Minimizing (9) for system (7) is equivalent to the original LQR problem (i.e. minimizing (4) for the original system (2)) — furthermore, this can be done by solving an LQR problem with system matrices (\tilde{A}, \tilde{B}) and cost matrices $\tilde{Q}, 0$. The resulting optimal controller is $\mu(t) = K\chi(t)$. This can be rewritten as

$$\mu(t) = K_0\delta_f(t) + K_1\gamma_1(t) + K_2\delta_r(t) \quad (10)$$

which, in conjunction with (5), make up the controller \mathcal{K} . We can convert these equations into z -domain to find that the transfer matrix $G(z)$ from $\Delta_f(z)$ to $\Delta_r(z)$ takes the following form:

$$G(z) = \frac{K_0}{z^2 - K_1z - K_2} \quad (11)$$

and has relative degree of 2. Thus, the controller obeys the form of the delayed controller in (3) for $T = 2$. The closed-loop system response to a pulse disturbance is shown in Figure 5. As expected, the controller responds with the appropriate amount of delay, and restores the force to equilibrium after the disturbance ends.

We now consider the resulting controller structure, shown in Figure 4, which has been studied in previous work [13], [15]. This structure has a net delay of $T = 2$, as specified. However, this structure is not compatible with the problem as specified. In particular, we specified that there is one timestep of communication delay from sensor to controller and from controller to actuator — this should translate to delays at the input and output of the controller. However, in Figure 4, the delays are in the middle of the controller as opposed to at the input and output. This serves as a motivating problem: we are interested in studying controllers that are compatible (to be made precise in the next section) with a particular delay structure.

Remark: The process shown in this section is one of three techniques for incorporating sensorimotor delays from previous work [13]. The two other techniques also suffer from the same issue of incompatibility.

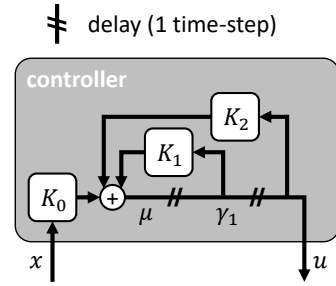


Fig. 4. Controller structure for the optimal delayed controller described by (5) and (10). Broken lines indicate one time-step of delay. This structure is not compatible with the specified communication delays.

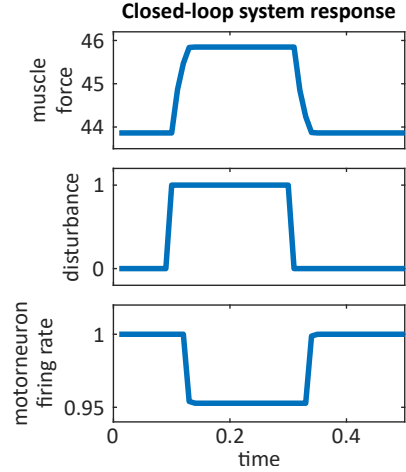


Fig. 5. Closed-loop system response to a unit pulse disturbance. Simulation parameters are provided in Section VI; equilibrium values are 1 for firing rate and 43.9 for muscle force. The control output (motorneuron firing rate) responds to the disturbance with a slight delay, and restores the force to equilibrium after the disturbance ends.

IV. COMPATIBILITY OF DELAYED CONTROLLERS

A. Realizations

We now review the standard concept of controller realizations. Let a controller be represented in z -domain as $G(z)$. A *realization* of a controller consists of matrices F, H, M, N such that $G(z) = M(zI - F)^{-1}H + N$. The state-space controller associated with this realization is written as:

$$\begin{aligned} x(t+1) &= Fx(t) + Hu(t) \\ y(t) &= Mx(t) + Nu(t) \end{aligned} \quad (12)$$

where we use x, u , and y to indicate the internal state, input, and output of the *controller* (as opposed to the plant). Every transfer function has infinite state-space realizations of varying size. If F, H, M, N are a realization for $G(z)$, then so are similarity transforms of the realization, i.e. $P^{-1}FP, P^{-1}H, MP, N$, where P is any invertible matrix. A *minimal realization* is a realization in which all eigenvalues of F are poles of $G(z)$; a *non-minimal realization* is a realization in F has more eigenvalues than $G(z)$ has poles.

B. Structure, delay graphs, and compatibility

We now introduce definitions of controller structures, delay graphs, and compatibility between the two.

Definition 1. The *structure* of a controller refers to the graphical representation of a specific realization of a controller. In this work, we will restrict graphical representations to only contain gain and addition blocks interconnected by scalar signals (possibly with delay).

If two controllers share the same graphical representation (e.g. the configuration of blocks are the same, even if the gain values are different), we say that they have the same structure. Structure depends on the sparsity pattern of the realization matrices rather than the numerical values of these matrices. Additionally, while every controller has infinite state-space realizations, different realizations can translate to the same structure. Overall, each controller can have multiple structures, and each structure can be associated with multiple controllers.

Definition 2. A *delay graph* is a directed graph with a source v_1 , sink v_N , and any number of intermediate vertices v_i , $i = 2 \dots N - 1$. Edge weights E_{ij} represent the delay (in timesteps) from vertex i to j . By convention, $E_{ii} = 0$. If vertex i does not directly communicate to vertex j , the edge weight is the sum of weights for the shortest path from i to j ; if no such path exists, the value is ∞ . The source v_1 represents the sensor that gives information to the controller; the sink v_N represents the actuator that receives input from the controller. Intermediate vertices and edges represent additional details and constraints on the internal structure of the controller.

The delay graph corresponding to the neuromuscular example is shown in the right side of Figure 2. This graph has $N = 3$ and a corresponding edge weight matrix

$$E = \begin{bmatrix} 0 & 1 & 2 \\ \infty & 0 & 1 \\ \infty & \infty & 0 \end{bmatrix} \quad (13)$$

Definition 3. For a given controller structure and delay graph, we can build a *delay assignment* describing relationships between signals in the controller structure and vertices in the delay graph. Each signal must be assigned to exactly one vertex; the input to the controller (u) must be assigned to v_1 , and the controller output (y) must be assigned to v_N .

A given controller structure can have multiple delay assignments, since multiple signal-vertex assignments are possible.

Definition 4. Every delay assignment has an associated *controller delay matrix*, denoted as \tilde{E} . \tilde{E}_{ij} indicates the delay along the fastest path from a signal at vertex i to a signal at vertex j . If no such signal exists, $\tilde{E}_{ij} = \infty$. By convention, $\tilde{E}_{ii} = 0$.

Definition 5. A given controller structure is *compatible* with a delay graph if there exists a delay assignment for this controller with an associated controller delay matrix \tilde{E} such that $\tilde{E}_{ij} \geq E_{ij} \quad \forall i, j$. Here, E is the edge weight matrix of the delay graph.

Definition 6. A given controller is *compatible* with a delay graph if at least one realization of the controller has an associated controller structure that is compatible with the delay graph.

The goal of these (somewhat long) definitions is to be able to rigorously assess whether a given controller could be implemented on a given system with some specific pattern of delays. A summary figure of these definitions and their relationships is given in Figure 6.

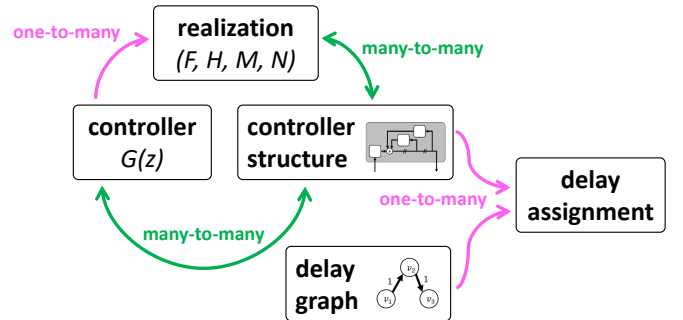


Fig. 6. Relationships between controllers, realizations, controller structures, delay graphs, and the delay assignment. Compatibility between a controller and a delay graph is assessed by comparing delay assignments associated with that controller to the delay graph.

As an example, consider the controller structure from Figure 4 and the delay graph in Figure 2. Let us try to build a compatible controller graph. Assign signal x to v_1 and signal u to v_N . The remaining signals to be assigned are γ_1 and μ . Notice that there exists a signal path (through the K_2 block) from u (at v_3) toward μ with no delay. If we assign μ to v_2 , this would mean $\tilde{e}_{32} = 0$; if we assign μ to v_1 , this would mean $\tilde{e}_{31} = 0$. In either case, compatibility is violated since $e_{31} = e_{32} = \infty$. The only option left is to assign μ to v_3 , but we notice that there exists a delay-free signal path (through the K_0 and addition blocks) from x (at v_1) to μ — this would mean that $\tilde{e}_{13} = 0$, which is again incompatible since $e_{13} = 2$. Therefore, this controller structure is not compatible with this delay graph, as there is no existing compatible controller graph. This makes our statements at the end of the previous section mathematically precise.

C. Creating a compatible delayed controller

We now consider the controller (11), which has many potential realizations and associated structures. We showed in the above subsection that one particular realization/structure is not compatible with the given delay graph. However, this does not preclude the possibility that other structures may be compatible — indeed, several compatible structures exist, which we now explore.

To ensure compatibility with the delay graph, we first split $G(z)$ into $G(z) = G_3(z)G_2(z)G_1(z)$, and enforce that $G_3(z)$ and $G_1(z)$ have relative degree 1. These correspond to the delays along e_{12} and e_{23} . Since $G(z)$ has relative degree 2, we see that the resulting $G_2(z)$ will have relative degree

0. Consider the simplest forms of $G_i(z)$:

$$G_1(z) = \frac{C_1}{z - \epsilon_1}, \quad G_3(z) = \frac{C_3}{z - \epsilon_3} \quad (14)$$

$$G_2(z) = \frac{K_0}{C_1 C_3} \frac{z^2 - (\epsilon_1 + \epsilon_3)z + \epsilon_1 \epsilon_3}{z^2 - K_1 z - K_2} \quad (15)$$

for some constants $C_1, C_2, \epsilon_1, \epsilon_2 \in \mathbb{R}$, $C_1 \neq 0$, $C_2 \neq 0$.

The realization for $G_i(z)$, $i = 1, 3$ is

$$x(t+1) = \epsilon_i x(t) + C_i u(t) \quad (16)$$

$$y(t) = x(t) \quad (17)$$

This is shown in Figure 7. This is compatible if we assign x , α_1 to v_1 , u to v_3 , and $\alpha_2, \alpha_3, \alpha_4$, as well as any internal variables in $G_2(z)$ to v_2 . Notice that even for this extremely simple first-order system, there are multiple possible structures — two such structures are shown in Figure 7. We choose the structure that, when combined with $G_2(z)$, produces a compatible structure.

The controller delay matrix associated with this assignment is:

$$\tilde{E} = \begin{bmatrix} 0 & 1 & \infty \\ \infty & 0 & 1 \\ \infty & \infty & 0 \end{bmatrix} \quad (18)$$

where \tilde{e}_{12} was determined by the signal from α_1 to α_2 , and \tilde{e}_{23} was determined by the path from α_4 to u .

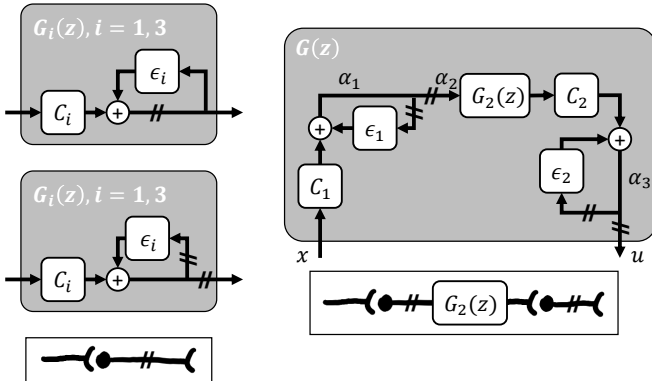


Fig. 7. (Left) Two controller structures associated with $G_1(z)$ and $G_3(z)$. We will use the structure on the bottom. (Right) Structure associated with $G(z)$. We also include (in outlined boxes) the neural circuit interpretation of each structure.

The general realization for $G_2(z)$ is

$$x_1(t+1) = F_{11}x_1(t) + F_{12}x_2(t) + H_1u(t) \quad (19)$$

$$x_2(t+1) = F_{21}x_1(t) + F_{22}x_2(t) + H_2u(t) \quad (20)$$

$$y(t) = M_1x_1(t) + M_2x_2(t) + Nu(t) \quad (21)$$

By rewriting $G_2(z)$ as

$$\frac{K_0}{C_1 C_3} + \frac{K_0}{C_1 C_3} \frac{(K_1 - \epsilon_1 - \epsilon_3)z + K_2 + \epsilon_1 \epsilon_3}{z^2 - K_1 z - K_2} \quad (22)$$

we see that $N = \frac{K_0}{C_1 C_3}$ for every realization.

We show the resulting structure in the left panel of Figure 9. This structure exhibits some symmetry between the upper and lower portions (e.g. the paths through H_1 and M_1 vs.

the paths through H_2 and M_2). Realizations with zeros will result in slight changes to the structure — for instance, the controllable canonical realization, in which

$$F = \begin{bmatrix} 0 & 1 \\ K_2 & K_1 \end{bmatrix}, \quad H = \begin{bmatrix} 0 \\ 1 \end{bmatrix} \quad (23)$$

$$M = \frac{K_0}{C_1 C_3} \begin{bmatrix} K_2 + \epsilon_1 \epsilon_3 & K_1 - \epsilon_1 - \epsilon_3 \end{bmatrix} \quad (24)$$

The resulting controller structure is shown in the left panel of Figure 10. We also have the observable canonical realization, in which

$$F = \begin{bmatrix} 0 & K_2 \\ 1 & K_1 \end{bmatrix}, \quad M = \begin{bmatrix} 0 & 1 \end{bmatrix} \quad (25)$$

$$H = \frac{K_0}{C_1 C_3} \begin{bmatrix} K_2 + \epsilon_1 \epsilon_3 \\ K_1 - \epsilon_1 - \epsilon_3 \end{bmatrix} \quad (26)$$

The resulting controller structure is shown in the left panel of Figure 11. As previously mentioned, the structure is partially dependent on the sparsity pattern in the realization matrices. To be precise, different sparsity patterns are necessary but not sufficient for different structures. For instance, if we switch the order of x_1 and x_2 for observable canonical realization, the resulting realization matrices would have different sparsity patterns, but the structure would remain the same.

V. NEURONS AND MICROCIRCUITS

It is unintuitive to attempt to compare controller structures with circuits of neurons. We now introduce a stylized “neuron”, which receives synaptic inputs (typically from the axons of other neurons) and produces an output on its own axon. The output of the neuron is a weighted combination of synaptic inputs and past outputs. We say that the neuron contains some *self-dynamics* because its output uses information from past outputs. Values of synaptic inputs and axon outputs represent firing rates. We can now use this stylized definition of a neuron to convert controller structural diagrams into “neural” circuits — an example is given in Figure 8. Axons can branch; the figure shows an axon with one branch, but an axon can split into multiple branches, allowing the output of the neuron to reach multiple downstream neurons. This is consistent with axon branching in neuroanatomy.

Our stylized neuron is similar to artificial neurons used in artificial neural networks for machine learning, with two key differences. Firstly, the self-dynamics in our neuron are conceptually reminiscent of a recurrent unit; secondly, our neuron lacks a nonlinear activation function. By avoiding this activation function, we are able to analytically and exactly translate controller structures to stylized neural circuits — we defer exploration of more complicated and realistic neurons to future work.

For each realization considered in the previous section, we draw the corresponding neural circuit — see the right panels of Figure 9 for the full realization, Figure 10 for the controllable canonical realization, and Figure 11 for the observable canonical realization associated with $G_2(z)$. Note

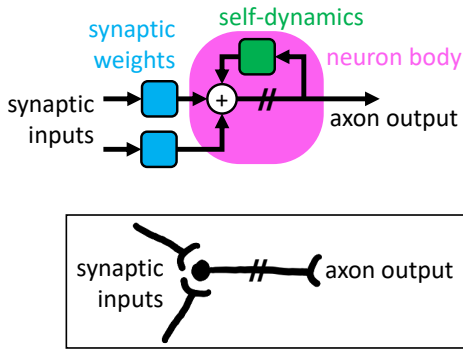


Fig. 8. A stylized neuron, depicted as a controller structure (top) and neural circuit (bottom). Squares in the top diagram represent scalar gains. The synaptic inputs are multiplied by the synaptic weights, and added to the self dynamics to produce the axon output (with some delay). The self-dynamics and computation occur in the “neuron body”. The neuron body is depicted by the circle in the lower diagram.

that the full circuit for $G(z)$ is simply the circuit for $G_2(z)$ plus an two extra neurons at the input and output (see bottom of Figure 7).

Additional simplifications to the different circuits for G_2 can be made if ϵ_i are selected such that $K_2 + \epsilon_1\epsilon_3 = 0$ or $K_1 - \epsilon_1 - \epsilon_3 = 0$ — this generally results in circuits that look like the controllable canonical realization (Figure 10), but with the middle neuron having only one axon branch instead of two.

Overall, we have three very distinct circuits, all of which — in conjunction with $G_1(z)$ and $G_3(z)$ — are compatible with the neuromuscular delay graph. It is interesting to see that although we have confined ourselves to minimal realizations, these minimal realizations translate to circuits with different numbers of neurons. Additionally, even though the controllable and observable canonical realizations have the same number of zeros in their matrices, they have circuits with different numbers of neurons (2 and 3, respectively).

These three circuits can be used to implement *any* second-order controller. This follows naturally from the generality of the three types of realizations we considered. This has interesting implications for neuronal circuits in the body — namely, that a given circuit can capture a wide array of behaviors depending on the specific values of the synaptic weights and self-dynamics. This is reminiscent of the idea of canonical microcircuits within the brain [20], in which the same circuit is found throughout the cortex (i.e. surface layer of the brain), and is hypothesized to perform some kind of universal computation. In our case, the “universal computation” associated with our circuits can be any second-order dynamical computation.

Remark: Some methods from [13] can be reworked such that the resulting controller structure is compatible with some sensorimotor delay graph, as is done in [21]. However, the resulting structure is highly non-minimal — indeed, for a scalar system, its dynamics can also be captured by one of the three circuits mentioned above.

VI. SIMULATIONS AND DISCUSSION

We perform numerical simulations to observe patterns of firing rates in the three circuits. We use the muscle model with parameters $\tau = 0.02$ seconds and $f_{\max} = 60$ N, taken from [17]. We linearize about non-negative values of motorneuron firing rate and muscle force, which represent values associated with some body equilibrium state². Let the one-way conduction delay between muscle and nervous system be 10 ms; we use step size of 10 ms. The resulting linear discrete-time system is described by (2) with $A = 0.61$ and $B = 4.64$. The net sensorimotor delay is $T = 2$ timesteps; the delay graph associated with the system is shown in Figure 2.

For each circuit, we plot the axon outputs of each neuron in response to a pulse disturbance. We include simulations with different parameters in $G_1(z)$, $G_2(z)$, and $G_3(z)$. Recall that these three transfer functions together make up the full controller — thus, the parameters for $G_1(z)$ and $G_3(z)$ will affect the numerical values of the $G_2(z)$ controller. Remember that all of these simulations correspond to the same controller output and closed-loop behavior, as shown in Figure 5 — however, each has a different circuit and/or neural firing pattern. We see that the firing patterns can vary even for a given circuit. For instance, for the full realization circuit, neuron x_1 ’s output can have a small change in firing rate (relative to equilibrium), or a large change in firing rate; additionally, the change can be positive or negative depending on the realization matrices’ values. Thus, given a sensorimotor system that behaves like an optimally controlled closed-loop system, we can provide plausible circuits and firing patterns that can implement the relevant optimal controller — however, we have no way of ascertaining which of the circuits and firing patterns are the correct ones (i.e. the circuit that is actually found in the nervous system). A key contribution of this work is to provide methods to generate plausible circuits, and to highlight the fact that circuits (and even behaviors within the same circuit) are non-unique. To find out which circuit is the correct one, we require data from the relevant biological neuron(s). Conversely, this means that if we are given data from biological neuron(s), we can tune the controller circuit to match this data while preserving the model’s match to behavioral observations.

VII. FUTURE WORK

In this work, we conducted a case study on a scalar neuromuscular system using linear neurons with self-dynamics. There are many directions of future investigation that would make this analysis more salient for neuroscience:

- 1) Incorporating more realistic features of neurons (e.g. nonlinear dynamics, thresholds, spiking)
- 2) Incorporating excitatory and inhibitory neurons. In animals, neurons are generally excitatory (i.e. all outputs of the neuron are associated with positive synap-

²Even when the body is at equilibrium, most muscle forces are not at zero; this is associated with some nonzero firing rate from the motorneuron. For instance, when standing, our leg muscles must maintain some constant force output, without which we would fall down

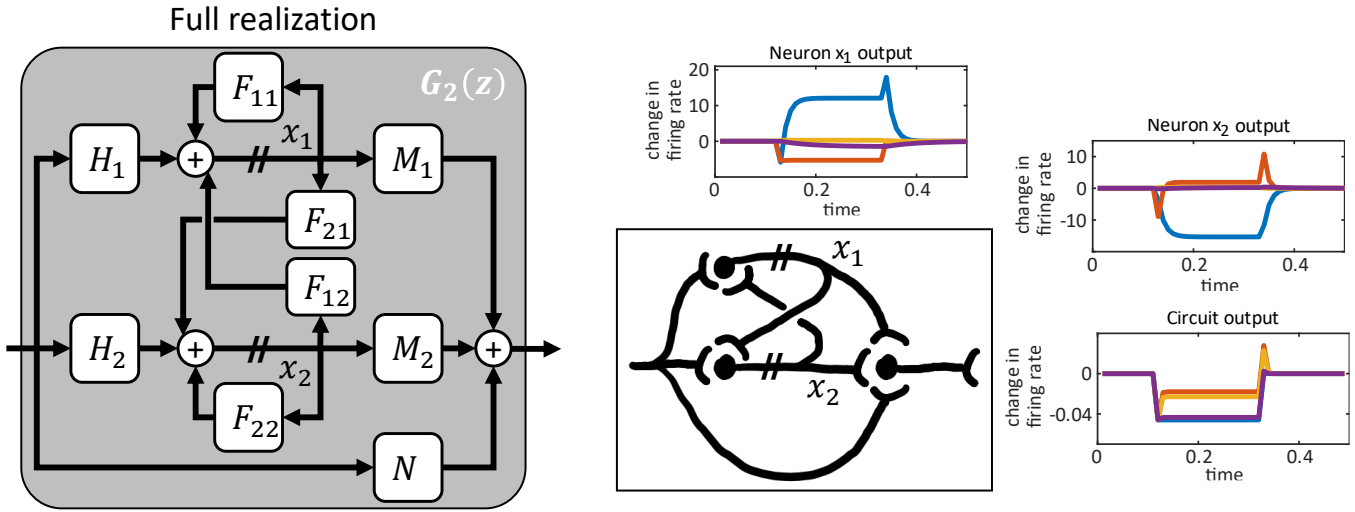


Fig. 9. (Left) Controller structure for $G_2(z)$ for a general realization. (Right) Neural circuit associated with this controller structure. Time-series of changes in firing rate (relative to equilibrium) are shown for four different simulations corresponding to different gain values (e.g. H_1 , H_2 , F_{11} , etc.)

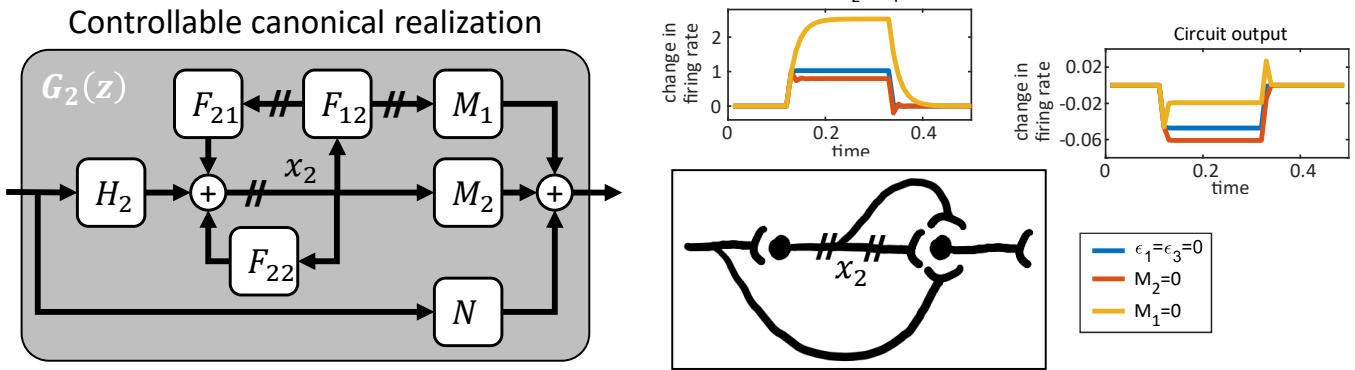


Fig. 10. (Left) Controller structure for $G_2(z)$ for the controllable canonical realization. (Right) Neural circuit associated with this controller structure. Time-series of changes in firing rate (relative to equilibrium) are shown for four different simulations corresponding to different gain values (e.g. H_2 , F_{21} , M_1 , etc.)

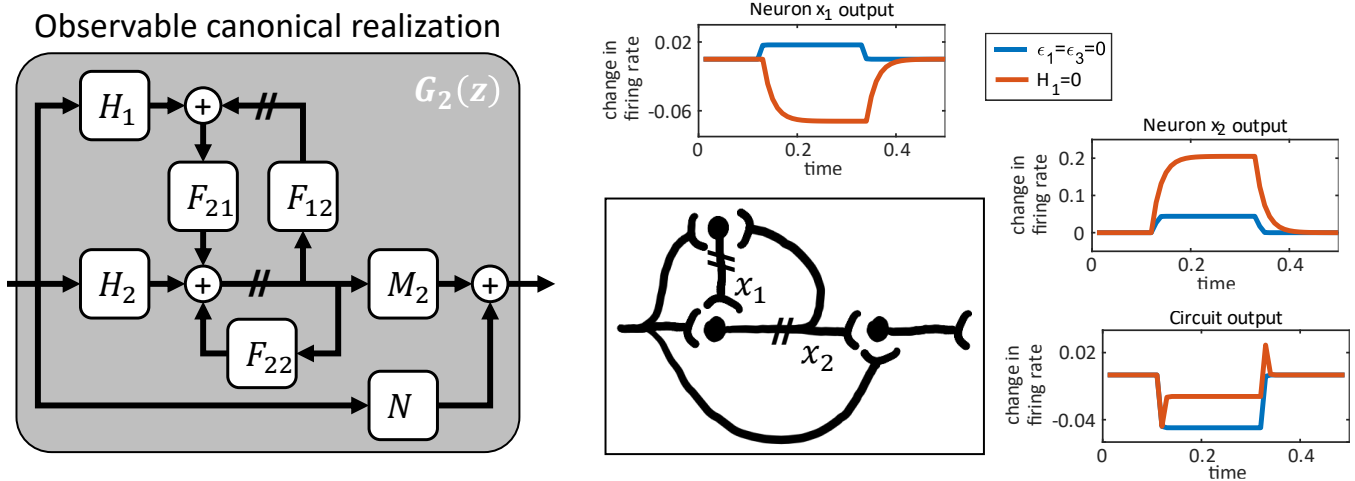


Fig. 11. (Left) Controller structure for $G_2(z)$ for the observable canonical realization. (Right) Neural circuit associated with this controller structure. Time-series of changes in firing rate (relative to equilibrium) are shown for four different simulations corresponding to different gain values (e.g. H_1 , H_2 , F_{21} , etc.)

tic weights on the downstream neuron) or inhibitory (i.e. all-negative synaptic weights). This translates to positivity requirements on internal variables in the controller realization and circuit structure

- 3) Investigating larger networks which process vector quantities instead of scalar quantities. For several model organisms (e.g. *C. elegans* and fruit flies), the entire network topology of the neurons within the nervous system is known; this network topology is referred to as a *connectome*. We can investigate how a given controller could be realized on a specific connectome or part of a connectome

REFERENCES

- [1] W. Li and E. Todorov, "Iterative linear quadratic regulator design for nonlinear biological movement systems," in *First International Conference on Informatics in Control, Automation and Robotics*, vol. 2, 2004, pp. 222–229.
- [2] S. H. Scott, "Optimal feedback control and the neural basis of volitional motor control," *Nature Reviews Neuroscience*, vol. 5, no. 7, pp. 532–545, 2004.
- [3] E. Todorov, "Optimality principles in sensorimotor control," *Nature Neuroscience*, vol. 7, no. 9, pp. 907–915, 2004.
- [4] D. W. Franklin and D. M. Wolpert, "Computational mechanisms of sensorimotor control," *Neuron*, vol. 72, no. 3, pp. 425–442, 2011.
- [5] M. Schultheis, D. Straub, and C. A. Rothkopf, "Inverse optimal control adapted to the noise characteristics of the human sensorimotor system," *Advances in Neural Information Processing Systems*, vol. 34, pp. 9429–9442, 2021.
- [6] S. H. Scott, "The computational and neural basis of voluntary motor control and planning," *Trends in cognitive sciences*, vol. 16, no. 11, pp. 541–549, 2012.
- [7] G. E. Loeb, "Optimal isn't good enough," *Biological cybernetics*, vol. 106, pp. 757–765, 2012.
- [8] R. C. Miall and D. King, "State estimation in the cerebellum," *The Cerebellum*, vol. 7, pp. 572–576, 2008.
- [9] T. DeWolf and C. Eliasmith, "The neural optimal control hierarchy for motor control," *Journal of neural engineering*, vol. 8, no. 6, p. 065009, 2011.
- [10] T. Bekolay, J. Bergstra, E. Hunsberger, T. DeWolf, T. C. Stewart, D. Rasmussen, X. Choo, A. R. Voelker, and C. Eliasmith, "Nengo: a python tool for building large-scale functional brain models," *Frontiers in neuroinformatics*, vol. 7, p. 48, 2014.
- [11] C. A. Goldsmith, N. S. Szczecinski, and R. D. Quinn, "Neurodynamic modeling of the fruit fly *drosophila melanogaster*," *Bioinspiration and Biomimetics*, vol. 15, no. 6, 2020.
- [12] R. Stagsted, A. Vitale, J. Binz, L. Bonde Larsen, and Y. Sandamirskaya, "Towards neuromorphic control: A spiking neural network based pid controller for uav," in *Robotics: Science and Systems*, 2020.
- [13] J. Stenberg, J. S. Li, A. A. Sarma, and J. C. Doyle, "Internal Feedback in Biological Control: Diversity, Delays, and Standard Theory," in *IEEE American Control Conference, 2022*, pp. 462–467.
- [14] J. S. Li, "Internal Feedback in Biological Control: Locality and System Level Synthesis," in *IEEE American Control Conference, 2022*, pp. 474–479.
- [15] J. S. Li, A. A. Sarma, T. J. Sejnowski, and J. C. Doyle, "Internal feedback in the cortical perception–action loop enables fast and accurate behavior," *Proceedings of the National Academy of Sciences*, vol. 120, no. 39, p. e2300445120, 2023.
- [16] J. W. Krakauer, A. A. Ghazanfar, A. Gomez-Marín, M. A. MacIver, and D. Poeppel, "Neuroscience needs behavior: correcting a reductionist bias," *Neuron*, vol. 93, no. 3, pp. 480–490, 2017.
- [17] P. Greene, A. J. Bastian, M. H. Schieber, and S. V. Sarma, "Optimal reaching subject to computational and physical constraints reveals structure of the sensorimotor control system," *Proceedings of the National Academy of Sciences*, vol. 121, no. 14, p. e2319313121, 2024.
- [18] H. L. More and J. M. Donelan, "Scaling of sensorimotor delays in terrestrial mammals," *Proceedings of the Royal Society B*, vol. 285, no. 1885, p. 20180613, 2018.
- [19] J. C. Tuthill and R. I. Wilson, "Parallel transformation of tactile signals in central circuits of *drosophila*," *Cell*, vol. 164, no. 5, pp. 1046–1059, 2016.
- [20] S. B. Nelson, "Cortical microcircuits: diverse or canonical?" *Neuron*, vol. 36, no. 1, pp. 19–27, 2002.
- [21] L. Karashchuk, J. S. L. Li, G. M. Chou, S. Walling-Bell, S. L. Brunton, J. C. Tuthill, and B. W. Brunton, "Sensorimotor delays constrain robust locomotion in a 3d kinematic model of fly walking," *eLife*, Aug. 2024.